Computed Tomography of Polymer Composites Reinforced with Natural Short Fiber

César Paltán[1], Josep Costa[2], and Jorge Fajardo[1(✉)]

[1] Universidad Politécnica Salesiana, Cuenca, Ecuador
jfajardo@ups.edu.ec
[2] AMADE, Polytechnic School, University of Girona, Girona, Spain

Abstract. X-ray computed tomography is a technique that provides a high level of detail in three-dimensional (3D) inspections of composite materials, but the acquisition of phase contrast together with absorption contrast in traditional tomography makes it difficult to obtain information in some composite materials reinforced with natural fibers. In this work, X-ray computed tomography has been used to evaluate an image reconstruction process using the phase-contrast method with three different algorithms (MBA, BAC, PPR). The results of the image reconstructions were compared to traditional methods. Additionally, details of the variation of parameters in each reconstruction method are presented. The phase-contrast image capture technique did not provide an adequate reconstruction of images that showed similar contrast. Finally, the absorption contrast was applied to analyze morphological properties of a bio-based composite showing a significant decrease of fiber length distribution during the manufacturing process.

Keywords: X-ray tomography · Phase contrast · Phase retrieval · Absorption phase · Modified Bronnikov Algorithm (MBA) · Paganin Phase Retrieval (PPR) · Bronnikov Aided Correction (BAC) · Bio-based composite

1 Introduction

In X-ray computed tomography (CT), a sample is inspected by taking a series of X-ray transmission images at different angles, since X-ray can be transmitted thought large composite components [1, 2]. These projection images hold data about the X-ray absorption coefficients of the different materials in the sample, and are used to obtain a 2D or 3D representation of the sample [2–4]. This technique is non-destructive [5], and is used to determine the internal structure of the materials (with a post process, the fiber length distribution (FLD) and the fiber orientation distribution (FOD) are measured, two critical parameters for the behavior of composite materials reinforced with short fiber) [6–8]. A typical X-ray computed tomography (CT) imaging procedure is composed of two steps: data acquisition and image reconstruction [9, 10].

It is known that there three different ways of doing an X-ray tomography. The absorption mode is presented by the variation between the linear attenuation

© Springer Nature Switzerland AG 2019
S. Misra et al. (Eds.): ICCSA 2019, LNCS 11623, pp. 452–467, 2019.
https://doi.org/10.1007/978-3-030-24308-1_37

coefficients, the greater the difference, the better the contrast and the easier the subsequent analysis of image [2, 11–13]. The phase contrast mode is observed when the distance between the detector and the sample increases in comparison with the absorption mode. The interference after the propagation between the wave on each side of an interface, generates the contrast because it has undergone a different phase delay [11, 13, 14]. This contrast is superimposed onto the conventional absorption contrast, especially when absorption only leads to weak contrast [12] and is important when edge detection is necessary. The increased distance between the detector and the sample extends the Fresnel Zone that covers the image, and this results in stronger edges in the material [11]. This zone is the space between the transmitter of a wave and a receiver [15, 16]. Holotomography mode uses images taken at various distances from the sample to the detector. By using a specific algorithm, the quantitative distribution of the optical phase can be recovered. With this mode, quantitative 3D analysis of the density in the material is feasible [11, 12].

When X-ray computed tomography is performed on a very low absorbing or low attenuation sample, the X-rays that pass through the sample undergo a phase shift [17–19]. This attenuation is a function of the density and thickness of the sample along with the X-ray wavelength [5, 12]. Low attenuation is results from the reduction of the intensity of an X-ray beam as it passes through the material. This is caused by absorption and can be affected by different factors, such as the energy of the beam and the atomic number of the sample [16]. Then, the contrast of the image depends on the attenuation of the X-ray beam due to the sample [5] and also on the Fresnel Zone that is affected by the variation of the distance from the sample to the receiver [15]. With these conditions, the projection images obtained contain not only absorption contrast but also phase contrast, such as in plastics and composites [5]. While images without a phase signal can be reconstructed very well, such mixed phase images complicate slice reconstruction.

For these cases, the phase contrast imaging technique is used since this method takes the phase shift as an image signal and provides a better contrast in different samples such as soft tissues and samples with a low atomic number. This results in an improvement of the edge in the projection images, which can be analyzed as a positive peak in the intensity next to a negative one (relative to the intensity of absorption) [3, 19]. Phase contrast imaging techniques have two advantages: first, light elements, which show poor contrast in absorption radiography, can be easily detected and second, phase contrast radiography helps to reduce the dose of radiation deposited on the object under investigation [4]. Phase contrast can be measured with different methods, such as interferometric techniques [20].

The best modality of image capture in the phase contrast method is cone beam computed tomography (CBCT), which efficiently scans three-dimensional isotropic high-resolution images [10]. Within the CBCT technique, there are four ways to analyze the passage of X-rays [2]. Propagation Based Imaging (PBI) is the simplest because an optical element in the beam is not required and the restriction on the spectral width is relaxed [18, 21]. PBI depends on the interference fringes that arise in the propagation of free space in the Fresnel Zone. This method is particularly good at improving the edge in the image and, therefore, is very suitable for fiber samples, foams and for locating non-homogeneities in metals [21].

After image capture, phase contrast reconstruction has three methods that use mixed projections containing absorption contrast and phase contrast, the Modified Bronnikov algorithm (MBA), the Bronnikov aided correction (BAC) and the Paganin phase retrieval (PPR). Although the presence of the phase signal makes the projections (and even the reconstruction) look sharper, the phase signal is highly unwanted since it causes serious artifices in the reconstructed slices and introduces edges which are not physically present in the scanned object [22, 23].

The aim of this work is to explore reconstruction algorithms that transform the 2D projections acquired into 3D stacks specifically designed to improve the contrast in samples where all the constituents have a similar absorption of X-ray (as is the case of natural fiber composites). In particular, there will be an in-depth analysis of phase contrast algorithms. The document begins with a brief theoretical introduction, highlighting the basic concepts of reconstruction algorithms. Secondly, the methodology used to perform the analysis of the algorithms with variation of parameters is described. Finally, the absorption contrast method is applied to analyze morphological properties of a bio-based composite after the process manufacturing.

2 Background

2.1 Material Parameters

This section describes the main properties with respect to the X-ray CT imaging of composites.

Linear Attenuation Coefficient (μ)
One of the parameters for the detection of contrast between the different constituents within the volume of interest, in this specific case between matrix and fibers. It is a constant that describes the incident attenuation fraction (interaction of radiation with matter [24, 25]) per unit of thickness of material. It is expressed numerically in units of cm^{-1} [12, 16, 26, 27]. It is necessary to know the attenuation coefficient of a sample to correct the auto-attenuation. The attenuation coefficient is usually determined using the ratio of transmitted gamma-ray intensities and incidents with well-collimated sources and detectors [28, 29]. If the chemical composition of a sample is known, it can be calculated using simple data [28, 30].

$$\mu(x, y, z) = K\rho\frac{Z^4}{E^3} \tag{1}$$

Where K is a constant, ρ is the material density, Z is the material atomic number and E the energy of the incident photons.

Calculating μ for the intensity of the beam at distance x (cm) within a material using the following equation [12, 26].

$$I_x = I_0 e^{-\mu x} \tag{2}$$

Where I_x is the intensity at depth of x (cm), I_0 is the original intensity, and μ is the linear attenuation coefficient [27]. Rearrange and take the log of both sides gives the equation for μ.

$$\mu = \frac{Ln\left(\frac{I_0}{I_x}\right)}{x} \tag{3}$$

The mass attenuation coefficient is a normalization of the linear attenuation coefficient per unit density of the material that produces a value that is constant for a given element or compound [27].

Refractive Index Decrement (δ)

The Refraction Index Decrement is calculated from the atomic scattering factors and the cross-sections of Compton and Rayleigh. The atomic scattering factors are based on experimental measurements of atomic photo-absorption. The measurements provide values for the imaginary part of the atomic scattering factor and the real part, which describes the scattering of the radiation when it interacts with the matter, is calculated from the absorption measurements using the integral Kramers-Kronig relationships [31].

The refractive index n, describes the interaction of X-rays with matter, this depends on the material and the X-ray energy [1].

$$n = 1 - \delta + i\beta \tag{4}$$

Where the imaginary part β describes the attenuation (absorption) and the real part δ the phase shift. For polymer composites, the range of X-ray energies generally used are 15–20 keV for synchrotron sources, with δ higher than β by orders of magnitude [1, 13].

2.2 Algorithms

This section briefly describes the main algorithms with respect to the Phase contrast mode.

MBA (Modified Bronnikov Algorithm)

This method describes a correction application to these mixed projections to eliminate the phase signal [3]. The algorithm extracts and converts the phase signal from the mixed projection image, which allow reconstructing the phase signal as an absorption signal [19].

The algorithm is based on the transport of intensity equation [32]. The intensity distribution $I_{\theta,z}(x, y)$ at a distance z from the sample and angle of rotation θ, for samples with weak absorption and distances d in the nearby Fresnel zone, is expressed as [3, 19, 25]:

$$I_{\theta,d}(x, y) = I_{\theta,0}(x, y)\left[1 - \frac{\lambda d}{2\pi}\nabla^2\phi_\theta(x, y)\right] \tag{5}$$

Where $I_{\theta,0}(x,y)$ is the absorption-contrast intensity measured at $z = 0$, λ is the X-ray wavelength and $\phi_\theta(x,y)$ is the phase function of the sample.

Based on the Eq. (5) a filter is derived which is applied to the original projection data. This problem can be partially corrected by adding a correction parameter to the filter [3, 19].

In this filter, a correction factor is added that allows the algorithm to be used without knowledge of the intensity distribution at a distance d from the object near the Fresnel zone $(I_{\theta,d}(x,y,\lambda))$, therefore not requiring an additional scan. The two-dimensional Fourier transform of this filter has the following form [3, 4, 19].

$$p(\xi,\eta) = Q_{cor} = \frac{1}{\xi^2 + \eta^2 + \alpha} \tag{6}$$

Where ξ and η are the spatial frequencies and α is a correction parameter dependent on absorption; the constant α is an MBA correction. Very small values of the constant leads to fuzzy results because it eliminates the phase edges. Higher values maintain the sharpness of the projection but cannot eliminate the phase edges in their entirety. The use of large constant values eliminates the filter.

Applying Eq. (6) to the original projection images, the phase signal is eliminated and the absorption signal is converted into a set of line integrals $\phi_\theta(x,y)$ that contain information about the phase coefficients φ of the sample:

$$\phi_\theta(x,y) = \int \varphi dL \tag{7}$$

BAC (Bronnikov Aided Correction)

This method reduces the phase signal in the mixed projection, resulting in an almost pure absorption contrast projection, which can be reconstructed without introducing phase contrast artifices. The phase signal is used to correct original projection images and obtain a pure absorption image from which the attenuation coefficients μ of the object can be reconstructed [33]. According to Eq. (5), it is possible to obtain the pure absorption image $I_{\theta,0}(x,y)$ of the mixed projection $I_{\theta,d}(x,y)$ when the function $\phi_\theta(x,y)$ is known:

$$I_{\theta,0}(x,y) = \frac{I_{\theta,d}(x,y)}{1 - \frac{\lambda d}{2\pi}\nabla^2\phi_\theta(x,y)} \tag{8}$$

For the proposed BAC algorithm, the original projection images are first filtered using the modified Bronnikov filter, which results in the approximate phase function $\tilde{\phi}_\theta(x,y,\lambda)$. Then the correction function $C_\theta(x,y,\lambda)$ is calculated as [3]:

$$C_\theta(x,y,\lambda) = 1 - \gamma \cdot \nabla^2\tilde{\phi}_\theta(x,y,\lambda) \tag{9}$$

Where the parameter γ allows to control the amplitude of the correction. The parameter (BAC correction) controls the amplitude of the phase correction that is performed. Finally, the original projections $I_{\theta,d}(x,y,\lambda)$ are divided by the correction

function $C_\theta(x, y, \lambda)$ to obtain the corrected projection $I^a_{\theta,d}(x, y, \lambda)$ that should now contain only the absorption signal [3].

PPR (Paganin Phase Retrieval)
The algorithm is based on the transport of intensity equation [17, 32] and assumes that the object under study is composed of a single material, that the object is homogeneous.

It uses parameters that are geometrical, such as Source Detector Distance (SDD), Source Object Distance (SOD) and pixel size. The parameters μ and δ represent the linear attenuation coefficient and the refractive index decrement of the sample [4, 26, 34], assumed to be homogeneous [35]. For non-homogeneous samples and samples with an unknown composition, these parameters can be derived by visual comparison. By using the fast Fourier transform in the numerical implementation, a fast-deterministic method is obtained for phase extraction from a single defocused image of a homogeneous object.

$$T(\boldsymbol{r}_\perp) = -\frac{1}{\mu}\log_e\left(\mathfrak{F}^{-1}\left\{\mu\frac{\mathfrak{F}\{M^2 I(M\boldsymbol{r}_\perp, z = R_2)\}/I^{in}}{R_2\delta|\boldsymbol{k}_\perp|^2/M + \mu}\right\}\right) \tag{10}$$

Here, $T(\boldsymbol{r}_\perp)$ is the projected thickness of homogeneous object in the plane in which the image is taken, I^{in} is the uniform intensity of the incident radiation. The inverse Fourier transform is denoted $\mathfrak{F}^{-1}$, $M = (R_1 + R_2)/R_1$ is the magnification of the image resulting from the illumination of point source.

3 Materials and Methodology

3.1 Materials

The base composite material of this work was developed by the GiMaT group, which is a PP/bamboo fiber at different compositions. Polypropylene with flow index (MFI) of 12 g/10 min, was used as a polymeric matrix. Bamboo fibers belongs to mesh number 60 according to ASTM E 11–95 were employed as natural reinforcement. They were previously dried at 110 °C for 2 h [36–38].

3.2 Experimental Tests of X-ray Micro-tomography

The inspection equipment consisted of an X-ray source (20 W and 5 μm maximum power and focal spot) and a 2400 × 2400-pixel detector. Both were manufactured by HAMAMATSU and assembled by Novadep Scientific Instruments. The energy used was 30 keV, the effective pixel size was 6 μm and 1100 projections were taken (1 integration per projection). The distance between the sample and the camera (SOD) was 98,560 mm.

3.3 Reconstruction by Phase Contrast Mode

Three methods were used for reconstruction. The first method (Modified Bronnikov Algorithm) uses Eq. (6) with variation in the MBA attenuation parameters $(\xi^2 + \eta^2)$ between 0.25 to 2. At each different attenuation, it has a sub variation between 0.25 to 1.25 of the MBA correction parameters (α).

The second method (Bronnikov Aided Correction) uses Eq. (9) with variation in the BAC correction (γ) between 0.0025 to 1.

The third method (Paganin Phase Retrieval) uses Eq. (10) with a Source Detector Distance (SDD) of 821.33 mm, Source Object Distance (SOD) of 98.560 mm and pixel size 0.05.

The linear attenuation coefficient (μ), with a mass attenuation coefficient of $\mu_m = 0.2707 \frac{cm^2}{g}$ and a density of $\rho = 0.2707 \frac{cm^2}{g}$, has a value of $\mu = \mu_m \cdot \rho = 0.251\,\text{cm}^{-1}$ for polypropylene [30].

The refractive index decrement (δ) with values of $\delta = 2.48897e^{-7}$ and $\beta = 7.3776e^{-11}$ for polypropylene [39], behaves as shown in Fig. 1.

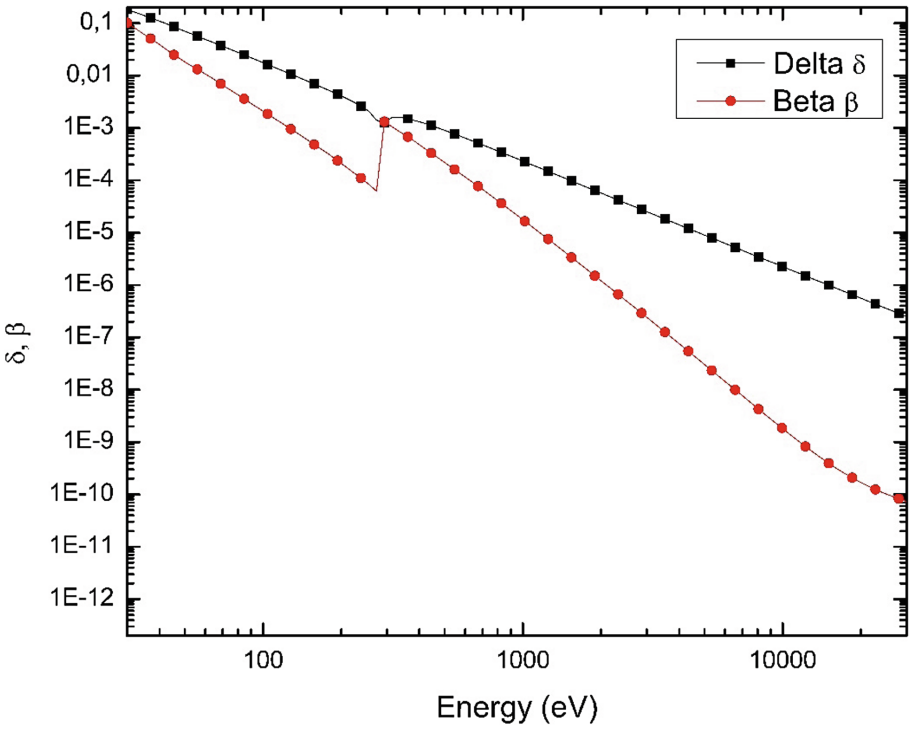

Fig. 1. Index refraction for polypropylene [39].

4 Results and Discussion

4.1 MBA (Modified Bronnikov Algorithm)

The first analysis shows the effect of the MBA algorithm with the variation of different parameters. The profile shows the transition between the edge of the fiber and the PP matrix shown in Fig. 2. As can be seen, the slices are different from each other. The slice image in Fig. 2(b) is very sharp with respect to the slice image in Fig. 2(a), but the reconstruction suffers from phase artifices. Because of these, the fiber, which is rather homogeneous, has a very dense edge and an internal region with a very high density that differs from the matrix.

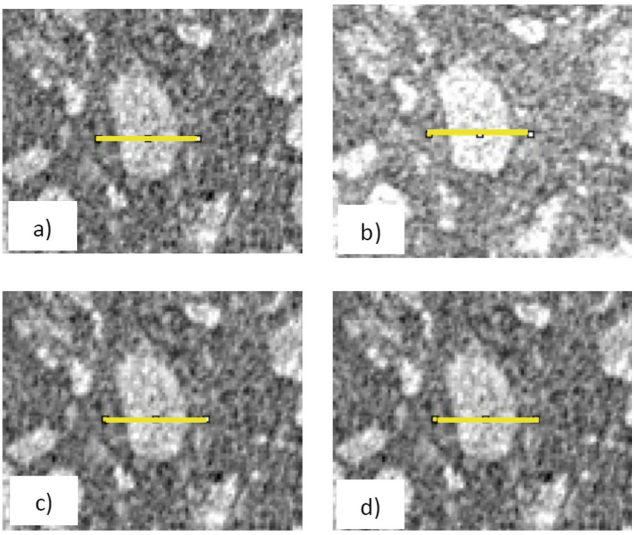

Fig. 2. (a) Original projection image. (b) Projection image after applying MBA (Modified Bronnikov Algorithm). (c) BAC (Bronnikov aided correction). (d) PPR (Paganin Phase retrieval).

Figure 3 shows a comparison of the line profiles for the original projection images and the MBA attenuation images at different values of this parameter. The profile shows the transition between the edge of the fiber and the PP matrix.

If the parameter is low (0.25 to 2), the peaks become smaller but do not disappear completely. If the parameters increase (>2), the peaks are similar to a normal reconstruction. For values that are lower (<0.25), the image loses a high amount of contrast and the edge is undetectable.

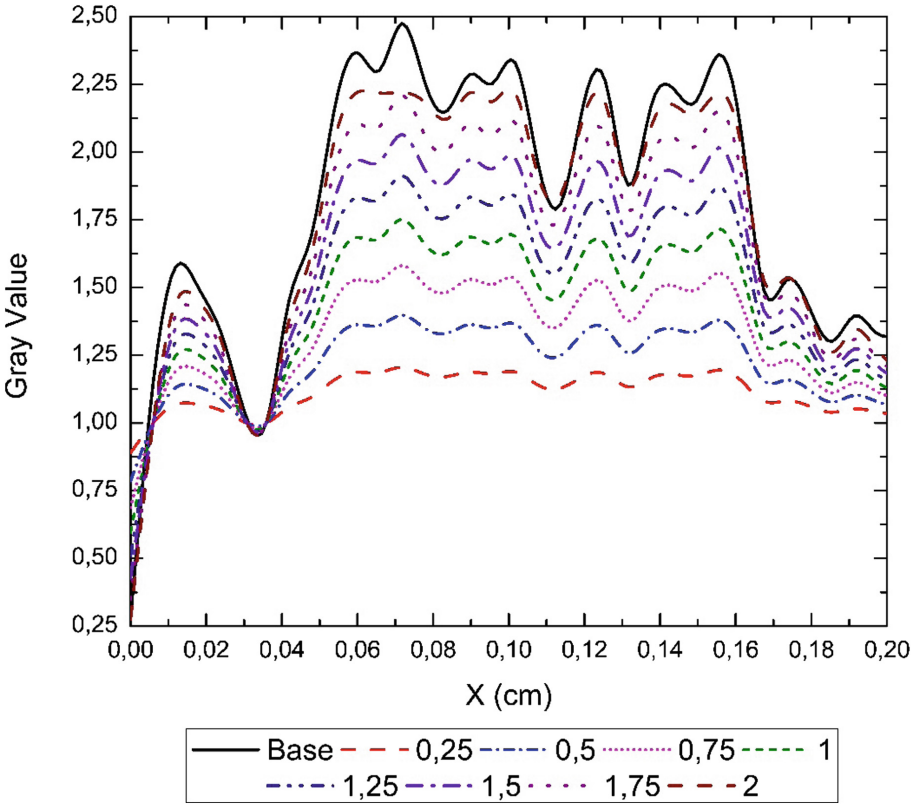

Fig. 3. Line profiles of the transition between the edge of the fiber with PP matrix for the original projection and for the MBA (Modified Bronnikov Algorithm) with different MBA attenuation parameter values and an MBA correction equal to 1.

Similarly, in Fig. 4, the line profiles of the original projection image and the MBA correction images are compared for different values of the MBA Correction parameter. The profile shows the transition between the edge of the fiber and the PP matrix.

With this parameter variation, no large changes are shown. If the parameter is low (0.25), the peaks are slightly reduced. If the parameter increases (>0.5), the peaks are similar to a normal reconstruction but remain under the original curve. As the parameter increases, there are no large-scale changes seen, with the curves of the parameter variation staying more or less the same. For values which are lower (<0.25), the image becomes blurred and the edge is not perceptible.

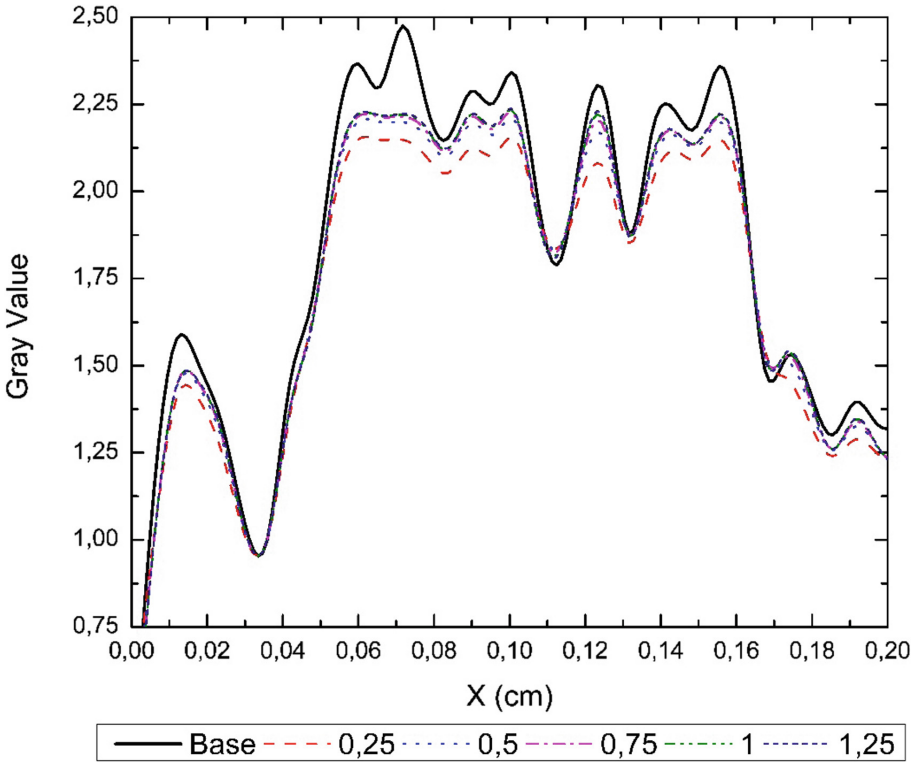

Fig. 4. Line profiles of the transition between the edge of the fiber with PP matrix for the original projection and for the MBA (Modified Bronnikov Algorithm) with different MBA correction parameter values and an MBA attenuation equal 1.

4.2 BAC (Bronnikov Aided Correction)

In the second analysis, the BAC slice, shown in Fig. 2(c), has little blurring as compared to the normal reconstruction shown in Fig. 2(a). The profile shows the transition between the edge of the fiber and the PP matrix.

In Fig. 5, the line profiles of the original projection and the BAC correction images are compared for different values of the parameter as it pertains to the behavior the BAC algorithm. If the parameter is very low (<0.0025), the peaks do not have significant changes (similar curves). As the parameter increases from (0.025 to 0.25), the peaks decreases with respect to normal reconstruction; the edge fades but not in its entirety. For lower values (>0.5), the image loses a high amount of contrast and the edge is undetectable.

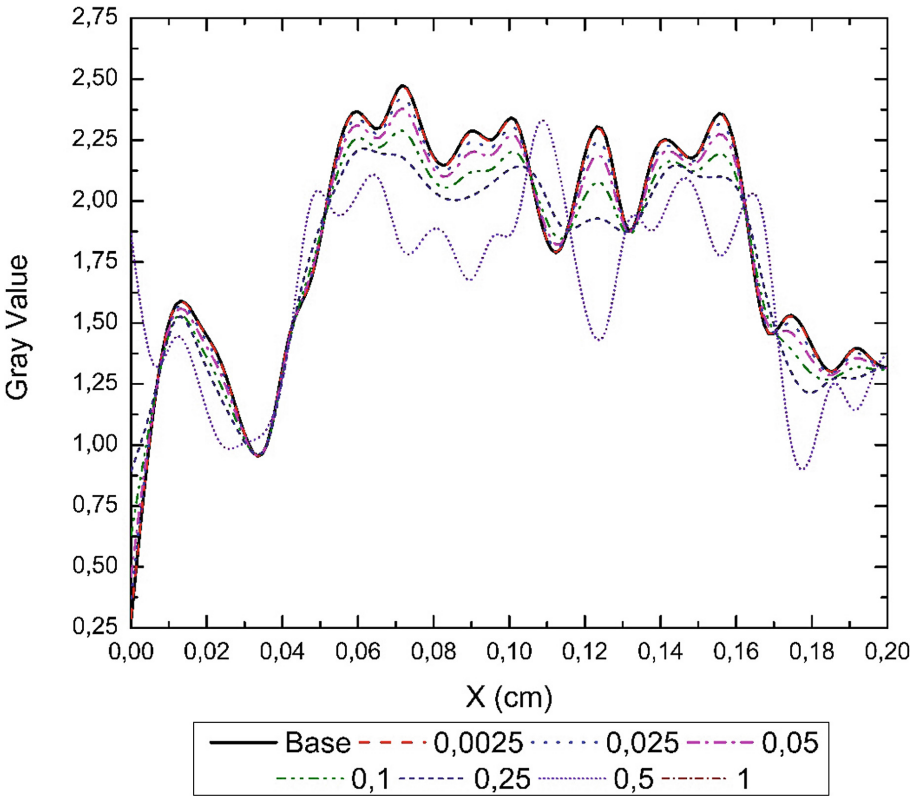

Fig. 5. Line profiles of the transition between the edge of the fiber and PP matrix for the original projection and for the BAC (Bronnikov Aided Correction) with different values for the BAC correction parameter.

4.3 PPR (Paganin Phase Retrieval)

Finally, the last analysis shows the effect of the PPR algorithm with the values of the properties of the PP Matrix. It is necessary to point out that in this reconstruction, the imaginary part of the refractive index parameter is used, the β factor, with results shown in Fig. 6. As can be observed, the peaks are similar to a normal reconstruction but under the original curve. When the real part of the refractive index parameter, the δ factor, is applied, the reconstruction that obtained is very blurred, with the edge is undetectable.

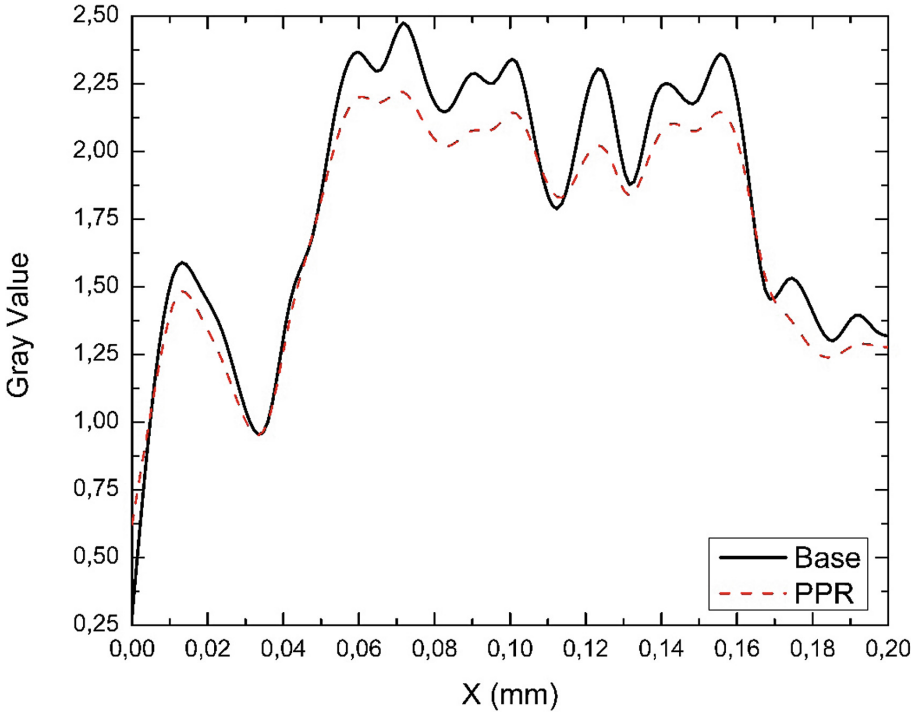

Fig. 6. Line profiles of the transition between the edge of the fiber with PP matrix for the original projection and for the PPR (Paganin Phase retrieval)

5 Case Study with Bio-Based Composite

In order to evaluate the method, a bio-based composite was developed from a thermoplastic matrix reinforced with natural fibers. Bamboo fibers with length 0.5 ± 0.1 mm, diameter 98.15 ± 0.1 μm, were used as reinforcement. Polypropylene homopolymer (PP), was used as a polymeric matrix. Composite materials at different formulations of bamboo (30 to 40 wt%) were manufactured. For the microstructural analysis of the bio-based composite, the X (μ-CT) was employed. With this technique it was possible to recreate images of the internal structure of the composite material and evaluate their microstructure (fiber length, diameter and orientation distribution). The images were acquired with a resolution of 6.5 μm using a voltage of 45 kV and current of 160 μA, by means of a Novadep micro-tomograph. The aspect ratio, diameter and length of the fibers were determined from 100 000 cross-sectional samples through the method developed by Miettinen et al. [40].

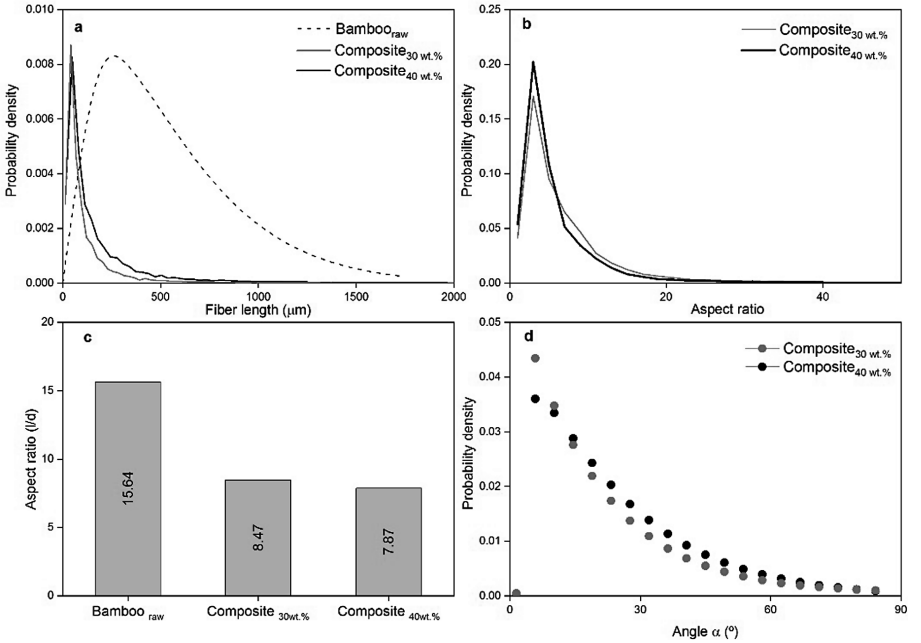

Fig. 7. Micromechanical parameters: (a) fiber length distributions, (b) aspect ratio distribution, (c) variation of the aspect ratio and (d) fiber orientation distributions.

Figure 7(a), shows a significant reduction of fiber length during processing. The fiber length distribution has been shifted towards the shorter fibers. The average fiber length before processing was ∼500 μm and after processing (extrusion + injection) it was reduced to 241 μm and 165 μm in the composite at 30 wt% and 40 wt% of bamboo fiber respectively. The aspect ratio of bamboo fiber was reduced by approximately half, due to the size reduction (Fig. 7b–c). The average fiber diameter before processing was found to be 33 μm, reduced to 28 μm and 21 μm at 30 wt% and 40 wt% of bamboo fiber respectively. Despite this effect, the average aspect ratio showed similar values in both compositions after processing (Fig. 7c). Figure 7(d), shows the fiber orientation distributions obtained from the weighted and averaged orientation distributions through the thickness of the specimens. The micromechanical information obtained from X (μ-CT) could be used together with micromechanical models to predict the mechanical behavior of these new materials.

6 Conclusions

The phase-contrast image capture technique proved not to offer a better method for the reconstruction of images, since the X-ray source does not have enough spatial coherence to increase the distance from the sample to the receiver and thus is not able to vary the Fresnel Zone. The captured images show only the absorption phase, which

is why the reconstruction algorithms (MBA, BAC, PPR) do not work in these cases. Normal reconstruction better maintains the detectability of the details showing a positive peak in the intensity next to a negative one. The BAC method is a technique for reconstructing mixed phase and absorption projections, since the method requires no additional combinations of parameters, projection data or prior information. The PPR method is a tool for analysis if the phase contrast is in the sample.

Acknowledgements. A grateful acknowledgement to the AMADE research group from the Universitat de Girona - Spain and the GiMaT research group from the Universidad Politécnica Salesiana – Cuenca, Ecuador for their support.

References

1. Garcea, S.C., Wang, Y., Withers, P.J.: X-ray computed tomography of polymer composites. Compos. Sci. Technol. **156**, 305–319 (2017)
2. du Plessis, A., le Roux, S.G., Tshibalanganda, M.: Advancing X-ray micro computed tomography in Africa: going far, together. Sci. Afr. **3**, e00061 (2019)
3. De Witte, Y., Boone, M., Vlassenbroeck, J., Dierick, M., Van Hoorebeke, L.: Bronnikov-aided correction for X-ray computed tomography. JOSA A **26**(4), 890–894 (2009)
4. Groso, A., Abela, R., Stampanoni, M.: Implementation of a fast method for high resolution phase contrast tomography. Opt. Express OE **14**(18), 8103–8110 (2006)
5. Stolidi, A.: High resolution X-ray phase contrast imaging for dynamic non-destructive testing of composite material. Paris-Saclay Ondes et Matière, Saclay
6. Shen, H., Nutt, S., Hull, D.: Direct observation and measurement of fiber architecture in short fiber-polymer composite foam through micro-CT imaging. Compos. Sci. Technol. **64**(13), 2113–2120 (2004)
7. Scott, A.E., Mavrogordato, M., Wright, P., Sinclair, I., Spearing, S.M.: In situ fibre fracture measurement in carbon–epoxy laminates using high resolution computed tomography. Compos. Sci. Technol. **71**(12), 1471–1477 (2011)
8. Wagner, P., Schwarzhaupt, O., May, M.: In-situ X-ray computed tomography of composites subjected to fatigue loading. Mater. Lett. **236**, 128–130 (2019)
9. Cai, W.: Feasibility study of phase-contrast cone beam CT imaging systems. Department of Physics and Astronomy, University of Rochester (2009)
10. Nasseh, I., Al-Rawi, W.: Cone beam computed tomography. Dent. Clin. North Am. **62**(3), 361–391 (2018)
11. Salvo, L., et al.: X-ray micro-tomography an attractive characterisation technique in materials science. Nucl. Instrum. Methods Phys. Res. Sect. B: Beam Interact. Mater. Atoms **200**, 273–286 (2003)
12. Barigou, M., Douaire, M.: 9 - X-ray micro-computed tomography for resolving food microstructures. In: Morris, V.J., Groves, K. (eds.) Food Microstructures, pp. 246–272. Woodhead Publishing, Sawston (2013)
13. Endrizzi, M.: X-ray phase-contrast imaging. Nucl. Instrum. Methods Phys. Res. Sect. A: Accelerators Spectrometers Detectors Assoc. Equip. **878**, 88–98 (2018)
14. Busse, G., Hemelrijck, D.V., Solodov, I., Anastasopoulos, A.: Emerging Technologies in NDT. CRC Press, Boca Raton (2008)
15. Chu, Y.S., et al.: Hard-X-ray microscopy with Fresnel zone plates reaches 40 nm Rayleigh resolution. Appl. Phys. Lett. **92**(10), 103119 (2008)

16. McKetty, M.H.: The AAPM/RSNA physics tutorial for residents. X-ray attenuation. RadioGraphics **18**(1), 151–163 (1998)
17. Paganin, D., Mayo, S.C., Gureyev, T.E., Miller, P.R., Wilkins, S.W.: Simultaneous phase and amplitude extraction from a single defocused image of a homogeneous object. J. Microscopy **206**(1), 33–40 (2002)
18. Taba, S.T., et al.: Toward improving breast cancer imaging: radiological assessment of propagation-based phase-contrast CT technology. Acad. Radiol. **26**, e79–e89 (2018)
19. Boone, M., De Witte, Y., Dierick, M., Van den Bulcke, J., Vlassenbroeck, J., Van Hoorebeke, L.: Practical use of the modified Bronnikov algorithm in micro-CT. Nucl. Instrum. Methods Phys. Res. Sect. B: Beam Interact. Mater. Atoms **267**(7), 1182–1186 (2009)
20. Momose, A., Takeda, T., Itai, Y., Hirano, K.: Phase–contrast X-ray computed tomography for observing biological soft tissues. Nat. Med. **2**(4), 473–475 (1996)
21. Jian, F.: Phase contrast computed tomography. In: Computed Tomography-Clinical Applications. InTech (2012)
22. Inside Matters, Octopus Reconstruction User Manual, 8.9.2 (2016)
23. Fu, J., Hu, X., Li, C.: X-ray differential phase-contrast tomographic reconstruction with a phase line integral retrieval filter. Nucl. Instrum. Methods Phys. Res. Sect. A: Accelerators Spectrometers Detectors Assoc. Equip. **778**, 14–19 (2015)
24. Gupta, M.K., Sidhu, B.S., Mann, K.S., Dhaliwal, A.S., Kahlon, K.S.: Advanced two media (ATM) method for measurement of linear attenuation coefficient. Ann. Nucl. Energy **56**, 251–254 (2013)
25. Bronnikov, A.V.: Theory of quantitative phase-contrast computed tomography. J. Opt. Soc. Am. A (JOSAA) **19**(3), 472–480 (2002)
26. Biswas, R., Sahadath, H., Mollah, A.S., Huq, M.F.: Calculation of gamma-ray attenuation parameters for locally developed shielding material: Polyboron. J. Radiat. Res. Appl. Sci. **9** (1), 26–34 (2016)
27. Priamo, J.M.F.: Linear attenuation coefficient—radiology reference article—Radiopaedia. org. Radiopaedia. https://radiopaedia.org/articles/linear-attenuation-coefficient. Consultado 01 June 2018
28. Byun, J.-I., Yun, J.-Y.: A calibration transmission method to determine the gamma-ray linear attenuation coefficient without a collimator. Appl. Radiat. Isotopes **102**, 70–73 (2015)
29. Midgley, S.M.: Measurements of the X-ray linear attenuation coefficient for low atomic number materials at energies 32–66 and 140 keV. Radiat. Phys. Chem. **72**(4), 525–535 (2005)
30. Suplee, C.: XCOM: Photon cross sections database. In: NIST, 17 September 2009. https://www.nist.gov/pml/xcom-photon-cross-sections-database. Consultado 13 June 2018
31. Kuznetsov, S.: X-ray optics calculator. http://purple.ipmt-hpm.ac.ru/xcalc/xcalc_mysql/refractive.php. Consultado 09 July 2018
32. Teague, M.R.: Image formation in terms of the transport equation. J. Opt. Soc. Am. A (JOSAA) **2**(11), 2019–2026 (1985)
33. Abramovitch, K., Rice, D.D.: Basic principles of cone beam computed tomography. Dent. Clin. North Am. **58**(3), 463–484 (2014)
34. Wilkins, S.W., Gureyev, T.E., Gao, D., Pogany, A., Stevenson, A.W.: Phase-contrast imaging using polychromatic hard X-rays. Nature **384**(6607), 335–338 (1996)
35. Yu, R.P., Kennedy, S.M., Paganin, D.M., Jesson, D.E.: Phase retrieval low energy electron microscopy. Micron **41**(3), 232–238 (2010)
36. Fajardo, J.I., Santos, J., Garzón, L., Cruz, L.J.: Factorial study of process parameters on the orientation state of injected bamboo fibre/polypropylene composite parts, Ottawa (2015)

37. Fajardo, J., Lasso, D., Paltán, C., López, L., Perguachi, D., Cruz, L.: Improving the processing and rheological properties of natural fibre/polypropylene composites (2015)
38. Mera-Moya, V., Fajardo, J.I., de Paula Junior, I.C., Bustamante, L., Cruz, L.J., Barros, T.: Semi-automatic determination of geometrical properties of short natural fibers in biocomposites by digital image processing. In: International Conference on Information Theoretic Security, pp. 387–396 (2018)
39. Index of Refraction. http://henke.lbl.gov/optical_constants/getdb2.html. Consultado 01 June 2018
40. Miettinen, A., et al.: Non-destructive automatic determination of aspect ratio and cross-sectional properties of fibres. Compos. Part A: Appl. Sci. Manuf. **77**, 188–194 (2015)